AIMS Materials Science, 9(1): 36–55.
DOI: 10.3934/matersci.2022003
Received: 09 September 2021
Revised: 08 November 2021
Accepted: 16 November 2021
Published: 27 December 2021

http://www.aimspress.com/journal/Materials

Research article

Modification of Takari natural sand based silica with BSA (SiO_2@BSA) for biogenic amines compound adsorbent

Johnson N. Naat[1,*], Yantus A. B Neolaka[1], Yosep Lawa[1], Calvin L. Wolu[1], Dewi Lestarani[1], Sri Sugiarti[2] and Dyah Iswantini[2,*]

[1] Chemistry Education Department, Faculty of Education and Teachers Training, Universitas Nusa Cendana, Kupang, East Nusa Tenggara, 85001, Indonesia
[2] Department of Chemistry, Bogor Agricultural University, Bogor, 16144, Indonesia

* **Correspondence:** Email: johnson_naat@staf.undana.ac.id, dyahprado@yahoo.co.id.

Abstract: The modification of Takari natural sand-based silica with bovine serum albumin/BSA (SiO_2@BSA) as an adsorbent for biogenic amines compounds has been successfully synthesized. The SiO_2@BSA was synthesized by using the batch method, then was characterized by using FTIR and SEM. Here, A typical BSA group was identified with the new formed namely C–N and C–H, and N–H. The SEM image shows the surface morphology in granular, non-uniform, rough, and agglomerated forms. Several parameters such as adsorbent dosages, pH, and contact time, shows this material was optimum for adsorption of BSA at pH 5 with adsorbent dosages is 0.1 g during 80 min of contact time. The mechanism adsorption of BSA in this material was found out by using six kinetics modeling, and thermodynamic studies. Here, the adsorption of BSA was fitted with pseudo-second-order kinetics. Furthermore, the thermodynamic studies show that adsorption of BSA is spontaneously and follows chemical adsorption.

Keywords: adsorption; bovine serum albumin; kinetics, silica; sand from Takari; thermodynamics

Abbreviations: q_e: Adsorbate concentration at equilibrium time (mg/g); q: Adsorbate concentration adsorbed at t time (min); k_1: Pseudo first-order rate constant (min^{-1}); k_2: Pseudo second-order rate

constant ($g \cdot mg^{-1} \cdot min^{-1}$); k_p: Intraparticle diffusion rate constant ($mg \cdot g^{-1} \cdot min^{-1/2}$); C: Constant of boundary layer thickness (mg/g); B: Desorption constant related to surface area coverage and chemisorption activation energy(mg/g); C_0: Initial concentration of adsorbate in solution (mg/L); C_t: BSA concentration in solution at time t (mg/L); V: Solution volume (mL); M: The adsorbent weight per liter of solution(g/L); q: The adsorption capacity at t time (mg/g); α: (<1) and k_0 are the constant (mL/g); K_{int}: Intraparticle diffusion rate constant; q_t: Capacity at t time; T: Is the time and 1/2 is the slope of the linear plot; K_f: Initial external mass transfer coefficient

1. Introduction

The Takari sand on the Timor island is one of the natural materials with high silica content and this is evident from the extraction results with purity level up to 97.8%, which is a good source [1]. Silica is used as an adsorbent because it is very inert [2], hydrophilic [3], has thermal stability, high mechanical properties [4], and is relatively inflated (rigid) in organic solvents compared to polymer resin solids [5,6]. Furthermore, it has a good pore geometry structure and surfaces chemical properties [7,8]. This material can also adsorb toxic heavy metals and organic compounds due to its silanol and siloxane groups which are the active side of silica [9]. However, silica gel has disadvantages such as having low effectiveness and surface selectivity. Therefore, it needs to be modified because of these drawbacks and can be conducted by designing molecules to form new surfaces on silica containing organic molecules using crosslinking agents as precursors [10,11]. One of the modifying agents is bovine serum albumin (BSA) [12–14].

BSA is a type of inert globular protein with a large mass dissolved in water, derived from humans [15,16] and egg whites [17–19]. It can be used as a modifying agent due to its biocompatibility, biodegradability, and heat resistance up to 60 ℃ for 10 h [16,20,21]. In addition, it is stable in the pH range 4–9 and has high solubility at pH 7.4 [16,22–24]. It also has good ligand connection properties making it eligible for use in silica modification [20,25,26], with good conformational adaptability [24]. This is evident in the study conducted by Mallakpour and Yazdan [27] which stated that the adsorption strength of silica by BSA increased more than 2 times and its thermal stability by about 37% [28].

The modification enables BSA to occupy parts of the silica to increase its ability to adsorb toxic organic compounds such as biogenic amines [29]. Biogenic amines are nitrogenous low molecular weight organic bases and they have an aliphatic, aromatic, or heterocyclic structure [16]. Biogenic amines are natural antinutritional factors and are important from a hygienic point of view as they have been implicated as the causative agents in some food poisoning episodes, and they can initiate various pharmacological reactions. Histamine, tyramine, tryptamine, β-phenylethylamine, and spermidine are considered to be the most important biogenic amines occurring in foods. These amines are designated as biogenic because they are formed by the action of living organisms [30]. Histamine has been implicated as the causative agent in several outbreaks of food poisoning, while tyramine and β-phenylethylamine have been proposed as the initiators of hypertensive crisis. Biogenic amines may also be considered carcinogens because of their ability to react with nitrites to form potentially carcinogenic nitrosamines [31].

The advantages of modifying silica with BSA involve using it in a continuous process to reduce production costs, stop reactions quickly, and control product formation [30–32]. Furthermore, silica

can be modified using BSA because there can be an interaction between the aminopropyl and the hydroxyl (–OH) group to form a hydrogen bond [33,34]. Some research on the silica-BSA modification was found the effect of its modification with BSA on the physicochemical properties of polyvinyl alcohol (PVA) [35,36], adsorption of biogenic amines using mobilized silica adsorbent BSA [9]. Joseph et al. [28] conducted a study by coating magnetic nanoparticles using BSA, and it was reported that the size Increased, and a corona structure was formed. Nairi et al. [37], studied this modification and the results showed an interaction between silica@BSA.

To understand the mechanism and dynamics of BSA adsorption modification on silica, equilibrium studies are necessary [38]. Several models of equilibrium and kinetics have been developed to conduct experimental designs, with various aspects of limitations on complex mechanisms [39]. In addition, parameters and adsorption model Kinetics are useful for obtaining information on the properties of the adsorbent surface, adsorption mechanism, adsorbate-adsorbent interactions, and intrinsic adsorption kinetics constant. The equilibrium approach is useful in understanding the thermodynamic aspects of the adsorption process [40]. Therefore, the characterization of synthesized silica@BSA will be reported using FTIR and SEM. Important parameters in the adsorption process include silica mass, optimum pH, and contact time. Also, the six kinetics model include PFO, PSO, Weber-Morris Intraparticle diffusion, Elovich, Bangham, and Diffusion-base kinetic models external diffusion, and the thermodynamic parameter values are ΔH^o, ΔG^o, ΔS^o, and ΔHx. These are the novelty of this study with the use of silica sourced from the Takari natural sands. The synthesized adsorbent will be used as an adsorbent candidate in adsorbing biogenic amines toxic compounds obtained from food ingredients.

2. Materials and methods

2.1. Materials

The material used includes Bovine Serum Albumin (heat shock fraction, ≥98% Sigma-Aldrich, USA), NaOH crystals pro analysis ≥99% (Merck KGaA-Germany), HCl pro analysis 37% (Merck ACS, ISO, Reag. Ph Eur), acetic acid Sigma Aldric (CH_3COOH, 100% (v/v)), KH_2PO_4 ACS Reagent ≥99%, Lowry-Folin-Ciocalteu reagent Merck obtained from Germany, Na_2CO_3 Sigma Aldrich, Natrium Kalium Tartrat ACS, ISO reagent and natural sand of Takari from Timor island-East Nusa Tenggara.

2.2. Silica extraction (SiO_2)

The procedure for the extraction of silica from natural sands was obtained from previous literature. 16 g of 200 mesh Takari sand powder dissolved in 240 mL 7 M NaOH and refluxed at 105 ℃ while stirring using a magnetic stirrer for 6 h until a mixture (sodium silicate) was formed. Meanwhile, the sodium silicate mixture was mixed with 240 mL of distilled water and allowed to stand for 24 h and separated through filtering. The filtrate was fitted with a 2 M HCl solution to a pH of 7 while continuing to stir until a white precipitate is formed. Also, it was left to stand at room temperature and washed using hot distilled water 5 times, filtered, and dried in an oven at 105 ℃ for 5 h and the

extracted silica gel was the white powder obtained [1,39,40].

2.3. Materials characterization

The instrument used was the Prestige-21 Shimadzu FTIR to determine the functional groups of silica and silica@BSA. Also, SEM brand FEI type Inspect-S50 was used to view surface morphological images. The determination of the BSA content of each sample complexed with Lowry-Follin reagent was conducted using Cary 3500 UV-Vis spectrophotometer.

2.4. Optimization of adsorption parameters

The SiO_2@BSA was synthesized by using the batch method. The mass and pH optimization were conducted with a variation of 0.04 to 0.2 g and from 3–10 respectively. The optimization of contact time varied from 30–100 min, and each treatment was interacted with 25 mL of BSA 10 mg/L solution and stirred for 80 min using a magnetic stirrer. Thereafter, the titrated solution was centrifuged for 10 min and filtered. It was taken as much as 1 mL and put in 8 mL of Lowry's reagent, left at room temperature for 10 min. 1 mL of Lowry-Folin reagent was added, shaken, and left for 20 min. Furthermore, the BSA content was measured using UV-Vis at a wavelength of 670 nm (optimum). To find out the percent of absorbed BSA, the formula in Eq 1 is used [27,41]:

$$\% \text{ Absorbed BSA} = \frac{(C_0 - Ce)}{C_0} \times 100\% \quad (1)$$

C_0 and C_e (mg/L) are the initial and equilibrium concentrations of BSA solution, respectively. To determine the adsorption capacity of BSA adsorbed at a certain time (q_e) (mg/L), it is calculated using Eq 2 [14,29,42]:

$$qe = \frac{(C_0 - C_t)V}{m} \quad (2)$$

Where C_0 is the initial concentration of the BSA solution (mg/L), C_t is the concentration of the analyte (BSA) at t time (min) (mg/L), V is the volume of the BSA solution used (L), and m is the mass of silica (g).

2.5. Adsorption kinetics

Determination of BSA adsorption kinetics was conducted by weighing 0.1 g of silica interacted with 25 mL of BSA 10 mg/L solution with variations in stirring time of 20, 40, 60, 80, and 100 min. This was conducted at optimum pH with a rotating speed of 300 rpm. The mixture was centrifuged for 10 min and the obtained filtrate was analyzed by UV-Vis. Six kinetics models were studied as shown in Table 1 and the results of the equation obtained a value close to 1. Therefore, the BSA adsorption model by silica follows the kinetics model.

Table 1. The mathematical model used to study BSA adsorption kinetics using silica adsorbent derived from Takari natural sand.

Kinetics Model	Linear shape	Graph plot	References
PFO	$\log(q_e - q_t) - k_1/2.303t + \log(q_e)$	$\log(q_e - q_t)$ vs t	[45,46]
PSO	$t/q_t = (1/q_e)t + 1/k^2q^2_e$	t/q_t vs t	[44,45,47,48]
Weber-Morris Intraparticle diffusion	$q_t = k_p t^{0.5} + C$	q_t vs $t^{0.5}$	[49–52]
Elovich	$q_t = 1/\beta \ln(\alpha\beta) + 1/\beta \ln(t)$	q_t vs lnt	[44,45,53–55]
Bangham	$\log\left(\log \frac{C_0}{C_0 - q_t.m}\right) = \log\left(\frac{k_0 m}{2.303\ V}\right) + \alpha \log t$	$\log\left(\log \frac{C_0}{C_0 - q_t.m}\right)$ vs log t	[44,45,53–55]
Diffusion-base kinetic model external diffusion	$\ln C_t/C_0 = -K_f(A/V)\ t\ [A/V = 3m/\rho d]$	In C_t/C_0 vs t	[56]

*Note: The symbol descriptions in table 1 can be seen in the nomenclature.

2.6. Adsorption thermodynamics

The variation in concentration from 10–50 mg/L BSA was used to determine the adsorption thermodynamics. This was conducted at a range of 10 at pH 5, volume 25 mL, stirred at 300 rpm for 80 min and controlled at 303 K. The obtained filtrate was measured by UV-Vis to determine the residual BSA concentration. Furthermore, the data obtained were processed and used to construct the curve ln ((X/m)/C_e) versus X/m. Based on the plot, a linear regression equation will be obtained with the intercept such as the Langmuir constant (KL), which is multiplied by the number 55.5 to obtain the value of the thermodynamic equilibrium constant (KC) [45]. The same procedure was conducted for temperatures of 303, 313, and 323 K and each variation will get a K value respectively. This value will be plotted between lnK versus 1/T, and from this plot, the values of ΔH^o and ΔS^o can be determined using the slope and intercept values. Meanwhile, ΔG^o can be calculated using Eq 3 [45,55–57]:

$$\Delta G^o = \Delta H^o - T\Delta S^o \quad (3)$$

The enthalpy and entropy change are calculated using Van't Hoff linear equation in Eq 4 [45,53]:

$$\ln k_d = \frac{\Delta S^\circ}{R} - \frac{\Delta H^\circ}{RT} \quad (4)$$

K is an equilibrium constant determined from the t plot intercept In q_e/C_e versus q_e, R is the ideal gas constant (8.314 $J \cdot mol^{-1} \cdot K^{-1}$), T is the absolute temperature (K). By plotting InK versus 1/T, the values of ΔS^o and ΔH^o can be determined from the slope and the intercept [58,59].

2.7. Isosteric adsorption heat (ΔH_x)

The isosteric enthalpy value can be obtained using thermodynamic adsorption data and substituting into Eq 5. A plot is made between the adsorbate concentration (C_e) versus 1/T, and from this plot can determine the value of ΔH_x through Eq 5 [45,60]:

$$(\ln C_e = \frac{\Delta H_x}{R\,T} + K) \quad (5)$$

K is the integration constant, C_e is the adsorbate concentration (mg/L), ΔH_x is the isosteric enthalpy (kJ/mol) and R is the ideal gas constant (8.314 $J{\cdot}mol^{-1}{\cdot}K^{-1}$). The heat of isosteric adsorption was calculated from the slope of the linear equation 1/T vs lnC_e.

3. Result and discussion

3.1. SiO_2@BSA characterization

The analysis results of the FTIR SiO_2 and SiO_2@BSA are shown in Figure 1. The spectra on the extracted silica showed a stretching vibration of OH at a wavelength of 3442.97 cm^{-1} originating from the active silica Si–OH group which decreased in silica@BSA to 3294.27 cm^{-1}. The study conducted by Timin et al. [29], showed the OH functional group appeared at 3482–3420 cm^{-1}. A new cluster was formed at a wavelength of 2956.13 cm^{-1}, and the C–H group was derived from the BSA. In the silika@BSA, there were 2 wave numbers 1651.61 cm^{-1} and 1535.34 cm^{-1}, respectively. They were the stretching of N–H amide vibrations and the C–N group on the silica surface due to the adsorption of C–N originating from BSA. This is consistent with Timin et al. [29] and Nairi et al. [37], where the strong peaks at around 1656 cm^{-1} and 1533 cm^{-1} are amide groups I and II usually close together. The numbers 1093.27 cm^{-1} and 795.75 cm^{-1} indicate the asymmetric and symmetrical stretching vibrations of Si–O on siloxane (Si–O–Si) [37].

In silica, the wavenumbers 1626.06 cm^{-1}, 1093.27 cm^{-1}, 789.18 cm^{-1}, and 464.65 cm^{-1} respectively showed the presence of –OH bending vibrations from silanol (= Si–OH), asymmetric stretching vibrations from the Si–O groups originating from the siloxane groups (Si–O–Si), symmetrical stretching vibrations from Si–O on the siloxane group (Si–O–Si) and the bending vibration of the siloxane group. The results of FTIR characterization showed the success of modified BSA which can be seen from the C–H, N–H, and C–N groups which are typical groups of BSA.

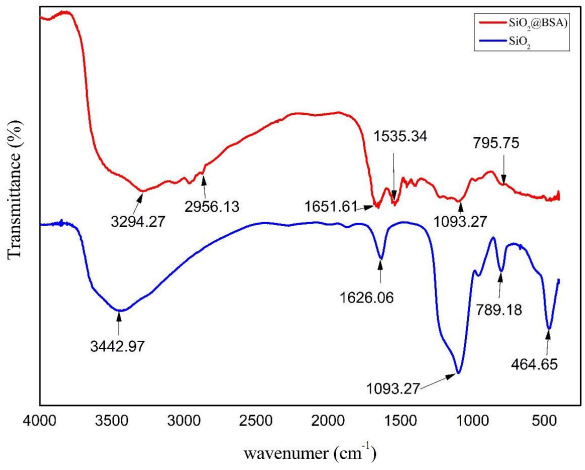

Figure 1. FTIR spectra of silica and silica@BSA.

3.2. *Silica@BSA surface morphology*

Analysis using SEM-EDX at magnifications of 5000×, 10000×, 20000×, and 50000× obtained clear information about the shape of the surface morphology of SiO_2@BSA, and the results of the surface morphology analysis are as shown in Figure 2.

Figure 2 shows silica and silica@BSA. The surface morphology of silica looks homogeneous with smaller particle sizes, in the form of evenly distributed granules. It shows that the surface of the silica@BSA adsorbent is in the form of imperfect grains with less homogeneous particle distribution, rough surface shape with hierarchical and agglomerated microstructure. The formation of larger (agglomeration) and non-uniform particle sizes in the analysis results show that there is a bond between silica and BSA. There is also an interaction between the hydroxyl on the silica with the COOH group and NH on BSA.

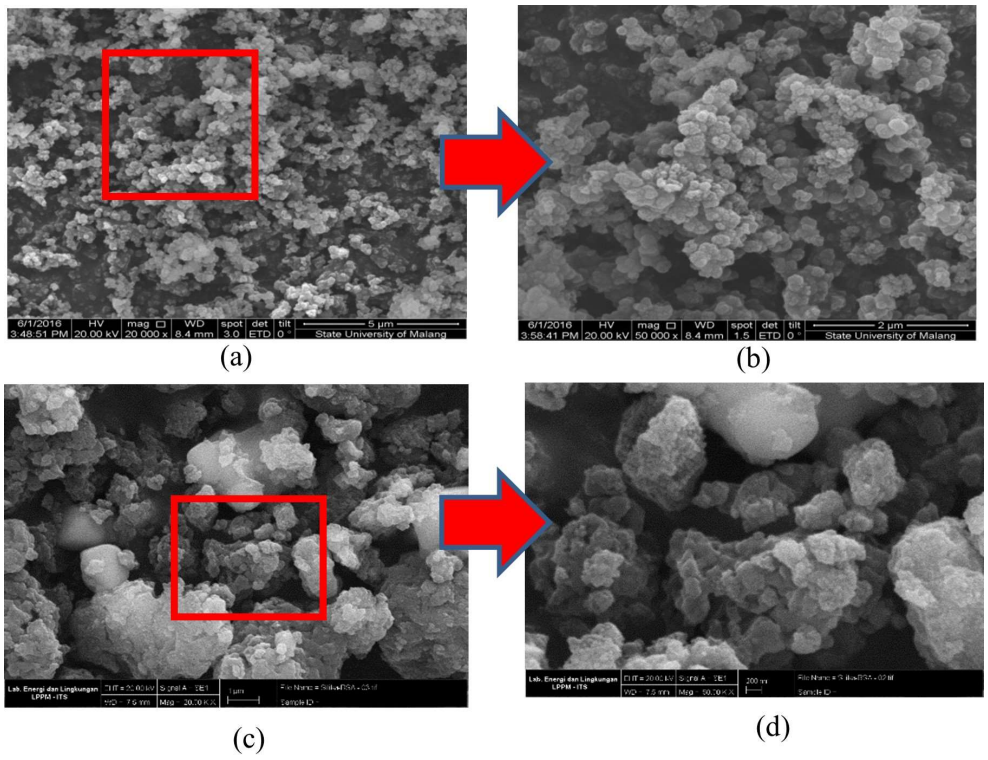

Figure 2. SEM Image of silica (a) 20.000× and (b).50.000×, SEM Image of SiO_2@BSA (c) 20.000×, (d) 50.000×.

3.3. Optimization parameters

3.3.1. Adsorbent mass optimization

The mass optimization curve resulting from silica immobilization with BSA measured using UV-Vis is presented in Figure 3. The curves obtained from the UV-Vis analysis showed that the optimum silica mass was 0.1 with an adsorption efficiency of 86% (q_e = 2.1 mg/g). Furthermore, the adsorbent mass of 0.04 to 0.1 g increases the amount of BSA adsorbed. This is because the adsorption

equilibrium factor on the silica surface has not been reached. However, at 0.2 g adsorbent mass, there was a decrease in the amount of adsorbed BSA. This is because, at 0.1 g adsorbent mass, the adsorption equilibrium was reached on the silica surface and has been filled with adsorbate molecules. Therefore, it is no longer possible for the adsorption process to occur.

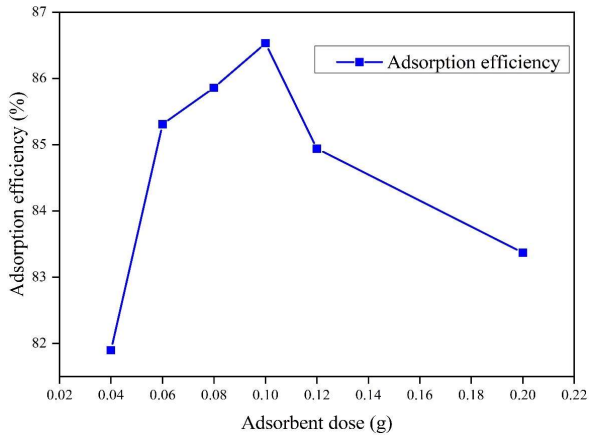

Figure 3. The adsorption efficiency curve is based on the adsorbent mass.

3.3.2. Optimum pH determination on BSA adsorption

This determination aims to obtain the optimum pH value for BSA adsorption on the silica matrix. This is because a pH value that is too low or high will make the adsorbent not work optimally [63]. The pH variations used were 3, 4, 5, 6, 7, 8, 9, and 10 and their selection followed the principle that aggregation, surface charge, coverage, and protein structure are investigated over the entire pH range [64]. The determination of the optimum pH using the UV-Vis Spectrophotometer is presented in Figure 4.

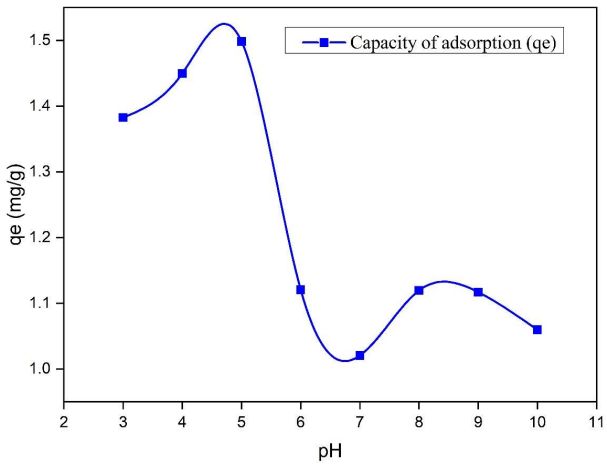

Figure 4. The curve of BSA adsorption capacity by silica.

Figure 4 shows that the optimum pH of BSA adsorption on the silica surface occurs at pH 5 and

the amount of the adsorbed substance is 1.498 mg/g. This is because the pH is close to the protein isoelectric point [24,63–65]. A large amount of aggregation, which occurs between particles from electrostatic interactions has decreased due to reduced stabilization of the charge [58]. Furthermore, in a solution that is not too acidic the amount of H^+ has decreased resulting in H^+ ions that do not bind to OH^- getting smaller. Therefore, this results in a greater chance of the aminopropyl group on BSA binding to the hydroxyl on silica. The high adsorption power of the adsorbent is caused by the bond formation mechanism, Van der Walls [64], hydrophobic and hydrophilic forces. The optimum pH is at pH 5 [29,64].

3.3.3. Determination of the optimal contact time

Determination of the optimum contact time is conducted to determine the best time in the BSA adsorption process on SiO_2@BSA. Also, in time optimization, variations of 30, 40, 50, 60, 70, 80, 90, and 100 min are used. The results of the analysis of determining the optimum contact time of BSA adsorption on the silica matrix using a UV-Vis spectrophotometer are presented in Figure 5.

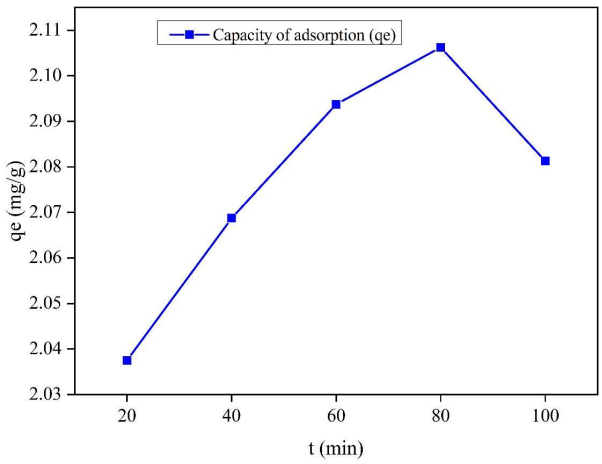

Figure 5. Optimum contact time curve.

Figure 5 shows the optimum time for BSA modification on the silica surface. The adsorbed BSA increase from the contact time of 30 to 80 min with an adsorption capacity of 2.106 mg/g. This is because the equilibrium factor on the silica surface has not been reached. When obtained, it can be seen that the adsorption curve has no longer increased because the process is not possible to occur in the adsorbent that has been filled with adsorbate molecules. However, it is possible to occur in the empty section [68]. Therefore, it can be concluded that at 80 min, the active site in the matrix silica has been filled by BSA and it does not allow adsorption. The capacity is estimated to be constant but at 90 since there is a decrease in the adsorption capacity. This is because at 90 min there is still BSA that will react with the active site. This free cationic activity causes the solution to become saturated and the bond to the active site of the adsorbent becomes weak. In addition, this results in the desorption of BSA molecules, which have been bound by the active site to be released causing the adsorbent pores to shrink back [69].

Table 2. Optimization data of BSA adsorption using silica from Takari.

Optimized parameters	Value	q_e (mg/g)
Mass of adsorbent (g)	0.1	2.150
pH	5	1.498
Contact time (min)	80	2.106

Notes: V=25 mL, T=25 ℃, C_0 = 10 mg/L, stirred with a shaker at 300 rpm

3.3.4. Adsorption kinetics of silica@BSA

BSA adsorption data on variations in contact time were analyzed using pseudo-first and second-order, Weber-Morris intraparticle diffusion, Elovich, Bangham, as well as external diffusion kinetics models. The graphs of each order are presented in Figure 6 and Table 3. The data in Table 3 and Figure 6 showed that the results of the BSA adsorption kinetics experimental test on silica adsorbent material have good suitability, which should be explained using a pseudo-second-order kinetics model. This can be considered following the high linearity of the relationship between the variables used. The value of the correlation coefficient R^2 obtained was 0.99 which indicates good suitability of the adsorption data with the second-order kinetics model [70].

Table 3. The values of the BSA adsorption kinetics parameter.

Kinetics models	Parameters
Pseudo first order	$R^2 = 0.014$
	$K_1 = -0.0062\ min^{-1}$
	$q_e = 0.041$ mg/g
Pseudo second order	$R^2 = 0.999$
	$K_2 = 0.964\ g \cdot mg^{-1} \cdot min^{-1}$
	$q_e = 2.105$ mg/g
Weber-Moris Intraparticle diffusion	$R^2 = 0.658$
	$K_p = 0.009\ mg \cdot g^{-1} \cdot min^{-1/2}$
	C = 2.003 mg/g
Elovich	$R^2 = 0.740$
	$\alpha = 0.061\ mg \cdot g^{-1} \cdot min^{-1}$
	$\beta = 28.571$ mg/g
Bangham	$R^2 = 0.740$
	$K_0 = 10\ mL \cdot g^{-1} \cdot L^{-1}$
Diffusion-base kinetic model external diffusion	$R^2 = 0.563$
	$K_f = 5.03 \times 10^{-6}$ cm/s

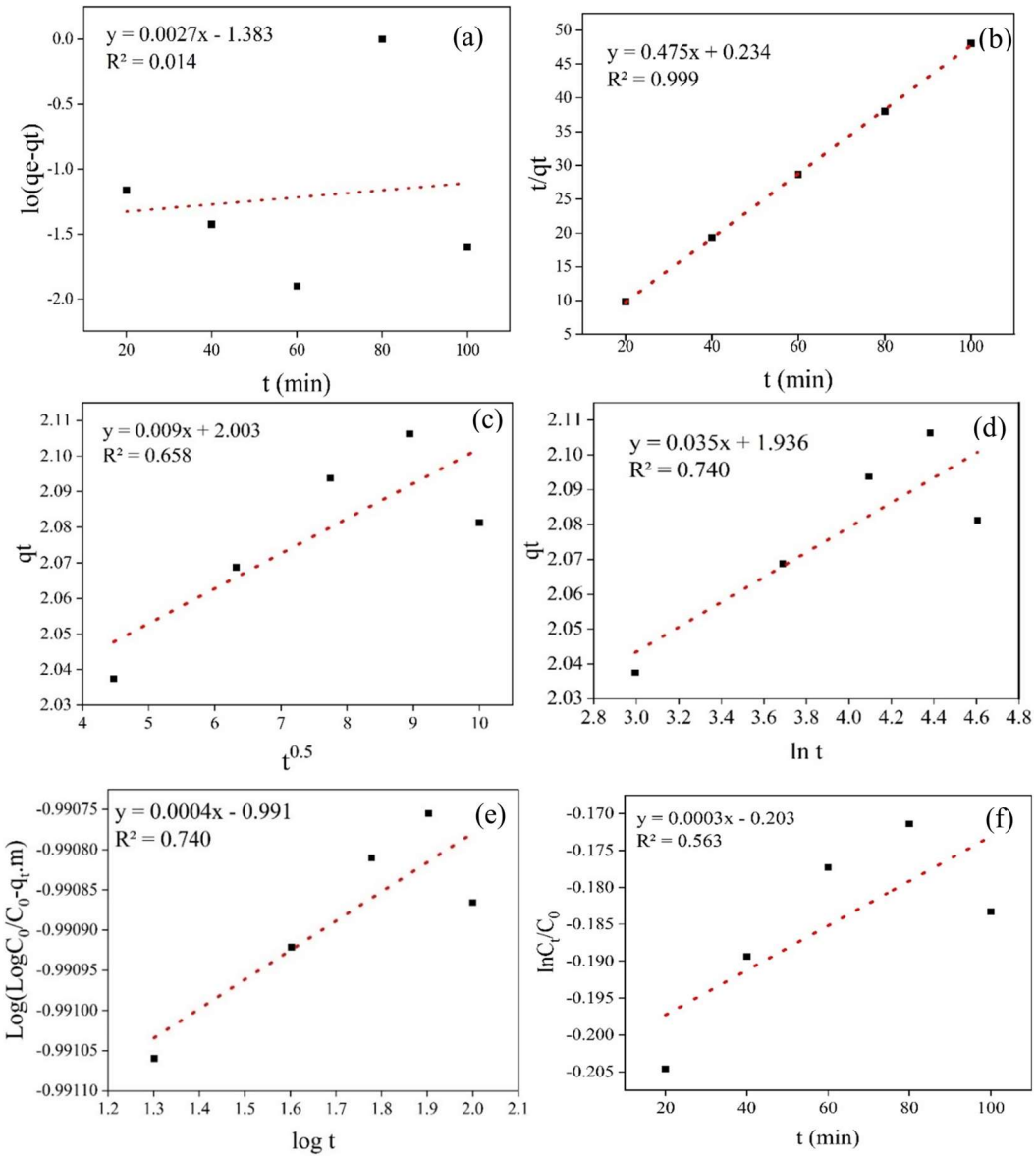

Figure 6. The curves of the adsorption kinetics model: (a) pseudo-first-order (PFO), (b) pseudo-second-order (PSO), (c) Weber-Morris intraparticle diffusion, (d) Elovich, (e) Bangham and (f) Diffusion-base kinetic model external diffusion.

Therefore, compared with others, it can be said that the second-order kinetics model will be able to provide the adsorption capacity value obtained from the experiment close. This may also be the following value obtained from theoretical calculations. The value of the equilibrium adsorption capacity obtained from the experiment (q_e = 2.106 mg/g) while that from the calculation of the pseudo-second-order kinetics model (q_e = 2.105 mg/g) [37,68]. These results indicate that BSA adsorption on silica occurs at certain localized active sites. Furthermore, there is the possibility of a chemisorption adsorption process with one of the mechanisms through the exchange of electrons between the adsorbent and BSA analyte [58]. Generally, the adsorbate binding process on the active side runs faster than a liquid layer or intraparticle diffusion [53] and does not limit the mass transfer process. The comparison of BSA adsorption by several studies is shown in Table 4.

Table 4. Comparison of several adsorbents on BSA adsorption.

Adsorbent	Kinetics models	References
TiO_2	Pseudo-first-order	[13]
Al_2O_3 and ZrO_2	Pseudo-first-order	[71]
DWNT	Pseudo-first-order	[14]
MWNT	Pseudo-first-order	[12]
Carbon	Pseudo-second-order	[72]
Silica from Takari	Pseudo-second-order	This work

3.3.5. Thermodynamic adsorption of silica@BSA

The study from the thermodynamic aspect uses several parameters such as changes in Gibbs free energy (ΔG^o), enthalpy (ΔH^o), and entropy (ΔS^o) [71]. Therefore, this study is needed to provide information relating to the direction and changes in internal energy within the adsorption process. The thermodynamic parameters of the adsorption are calculated based on the value of the equilibrium constant (Kc) obtained from each temperature variation. The value of lnKc is then plotted against 1/T following the linear form of the Van't Hoff equation. Therefore, the curve is obtained as shown in Figure 7. ΔG^o, ΔS^o and ΔH^o value obtained from the analysis is presented in Table 5.

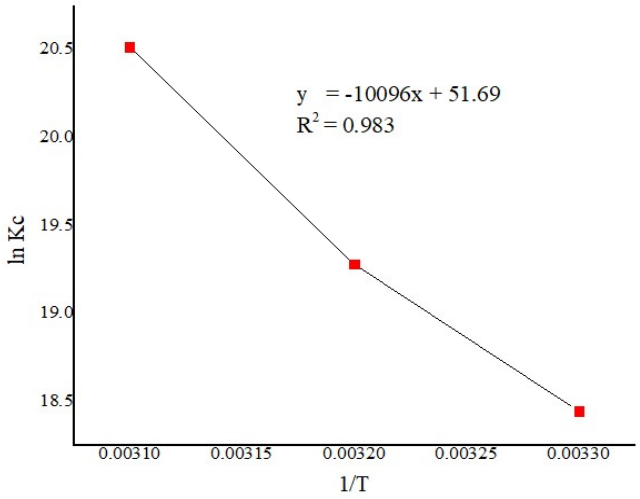

Figure 7. Van't Hoff curve (1/T vs InKc) of BSA adsorption by Takari natural sand-based silica adsorbent.

Table 5. The thermodynamic parameter values of BSA adsorption using silica.

Temperature (K)	ΔG^o (kJ/mol)	ΔH^o (kJ/mol)	ΔS^o ($J \cdot mol^{-1} \cdot K^{-1}$)
303	−46.276		
313	−50.573	83.938	0.429
323	−54.871		

Table 6 shows that the BSA adsorption process runs endothermically and was explained that the phenomenon of its capacity increases with increasing temperature [70]. The enthalpy data obtained showed that the BSA adsorption process happens chemically with the possibility of the dominant relationship type between adsorbate and the adsorbent through chemical interactions [37,68]. The small entropy (ΔS^o) value of 0.429 kJ/mol indicates a decrease in irregularity on the silica surface during the adsorption process. Consequently, it showed the suitability of the BSA adsorbate with the active site of the silica adsorbent and the presence of good adsorption reversibility [37,68]. Furthermore, the negative Gibbs free energy (ΔG^o) value showed that the adsorption process happens spontaneously at the optimum temperature (303 K) [39]. The result from Table 5 concluded that the BSA adsorption process on silica adsorbent occurs endothermically and spontaneously at 303 K, with chemical adsorption.

Table 6. Comparison of the thermodynamic parameter values of BSA adsorption with several adsorbents.

Adsorbent	ΔH^o (kJ/mol)	ΔS^o (kJ/ K·mol)	Adsorption Model	References
DWNT	9.40	321.5	Physisorption	[14]
MWNT	14.3	30.8	Electrostatically	[12]
Gold nanoparticle	8110.4	23.2	Chemisorption	[61]
Silica from Takari	83.938	0.429	Chemisorption	This work

3.3.6. Isosteric heat of adsorption (ΔH_x)

Another important thermodynamic parameter involving the amount of adsorbate adsorbed under constant conditions is the isosteric heat of adsorption. This parameter is an indicator for the profile of the separation process, which occurs by adsorption and the energy heterogeneity on the adsorbent surface. It can be determined using the chemical equilibrium thermodynamic approach. The calorific value of isosteric adsorption can be calculated from the slope of the linear equation 1/T vs $\ln C_e$ as seen in Figure 8. The isosteric enthalpy value obtained on BSA adsorption using silica adsorbent is represented in Table 7.

Table 7. BSA adsorption isosteric heat on silica.

Initial concentration (mg/L)	y = bx + a	ΔH_x (kJ/mol)	K-contant	R^2
10	y = −6339.3x + 17.992	−52.705	17.992	0.9592
20	y = −5634.4x + 16.641	−46.844	16.641	0.8412
30	y = −4407.5x + 13.207	−36.644	13.207	0.6888
40	y = −1357x + 3.9502	−11.282	3.9502	0.8834
50	y = 1158.8x−3.6369	9.634	−3.6369	0.9359

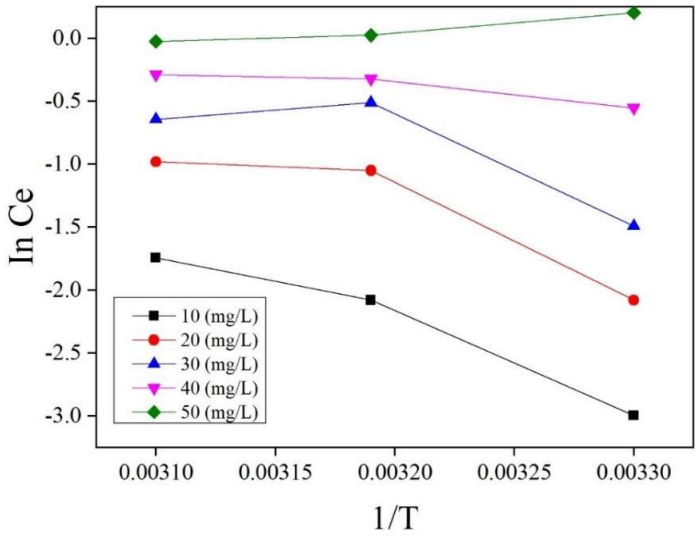

Figure 8. Isosteric curve in C_e for BSA adsorption using silica adsorbent at constant adsorbed amount as a function of 1/T.

The isosteric enthalpy value in BSA adsorption using silica adsorbent is strongly affected by the amount of adsorbate. This is because the isosteric enthalpy value tends to decrease with the increasing number of BSA. The variation of the enthalpy value showed that the degree of adsorbent heterogeneity is low. Furthermore, the high isosteric enthalpy value during the BSA adsorption process on the silica adsorbent takes place endothermically. The adsorbent surface shows that the interaction between BSA and silica adsorbent can happen optimally. This is because the surface of the silica adsorbent still contains active groups such as silanol and siloxane.

4. Conclusion

Takari natural sand-based silica was successfully modified with BSA (SiO_2@BSA), which is a new material for adsorbing toxic biogenic amines. BSA modification on the silica surface is conducted by studying several parameters such as characteristics, parameter optimization, kinetics, and thermodynamics. FTIR results showed a decrease in the wavelength of the OH functional group in silica from 3442.97 cm^{-1} to 3294.27 cm^{-1}. Furthermore, a new typical BSA group was formed, namely C–N, C–H, and N–H. The SEM image shows the surface morphology of silica@BSA is granular, non-uniform, rough, and agglomerated. The optimum mass of the adsorbent is 0.1 g with an adsorption efficiency of 86% and the optimum pH of BSA adsorption by silica is at pH 5 with q_e = 1.498 mg/g. The contact time is 80 min with q_e = 2.106 mg/g. Also, BSA adsorption kinetics followed the pseudo-second-order model with R^2 value and rate constant of 0.99 and 0.96 $g \cdot mg^{-1} \cdot min^{-1}$, respectively. Thermodynamic parameters of adsorption at ΔH^o = 83.938 kJ/mol, ΔG^o = −46.276, −50.574, and −54.871 kJ/mol, ΔS^o = 0.429 $kJ \cdot mol^{-1} \cdot K^{-1}$ and ΔH_x = −52.705, −46.844, −36.644, −11.282, and 9.634 kJ/mol indicates that the BSA modified silica process occurs endothermically, spontaneously through and chemical adsorption.

Acknowledgment

The author is grateful to the "Kementerian Pendidikan, Kebudayaan, Riset dan Teknologi" for supporting funds through the "Penelitian Kerja Sama antar Perguruan Tinggi (PKPT)" scheme.

Conflict of interest

All authors declare no conflicts of interest in this paper.

References

1. Naat JN, Lapailaka T, Sabarudin A, et al. (2018) Synthesis and characterization of chitosan-silica hybrid adsorbent from the extraction of timor-east Nusa Tenggara island silica and its application to adsorption of copper(II) ion. *Rasayan J Chem* 11: 1467–1476. https://doi.org/10.31788/RJC.2018.1144055
2. Ingrachen-Brahmi D, Belkacemi H, Mahtout ABL (2020) Adsorption of Methylene Blue on silica gel derived from Algerian siliceous by-product of kaolin. *J Mater Environ Sci* 11: 1044–1057.
3. Huang W, Xu J, Tang B, et al. (2018) Adsorption performance of hydrophobically modified silica gel for the vapors of n-hexane and water. Adsorpt. *Sci Technol* 36: 888–903. https://doi.org/10.1177/0263617417728835
4. Curdts B, Pflitsch C, Pasel C, et al. (2015) Novel silica-based adsorbents with activated carbon structure. *Micropor Mesopor Mat* 210: 202–205. https://doi.org/10.1016/j.micromeso.2015.02.007
5. Parida SK, Dash S, Patel S, et al. (2006) Adsorption of organic molecules on silica surface. *Adv Colloid Interfac* 121: 77–110. https://doi.org/10.1016/j.cis.2006.05.028
6. Sulastri S, Kartini I, Kunarti ES (2011) Adsorption of Ca(II), Pb(II) and Ag(I) on sulfonato-silica hybrid. *Indones J Chem* 11: 273–278. https://doi.org/10.22146/ijc.21392
7. Liu D, Lipponen K, Quan P, et al. (2018) Impact of pore size and surface chemistry of porous silicon particles and structure of phospholipids on their interactions. *ACS BiomaterSci Eng* 4: 2378–2313. https://doi.org/10.1021/acsbiomaterials.8b00343
8. Žid L, Zeleňák V, Almáši M, et al. (2020) Mesoporous silica as a drug delivery system for naproxen: Influence of surface functionalization. *Molecules* 25: 6–8. https://doi.org/10.3390/molecules25204722
9. Vlasova NN, Markitan OV, Golovkova LP (2011) Adsorption of biogenic amines on albumin modified silica surface. *J Colloid Interface Sci* 73: 26–29. https://doi.org/10.1134/S1061933X1006102X
10. Dash S, Mishra S, Patel S, et al. (2008) Organically modified silica: Synthesis and applications due to its surface interaction with organic molecules. *Adv Colloid Interfac* 140: 77–94. https://doi.org/10.1016/j.cis.2007.12.006
11. Pawlaczyk M, Kurczewska J, Schroeder G (2018) Nanomaterials modification by dendrimers–A review. *WJRR* 5: 14–30.
12. Bozgeyik K, Kopac T (2016) Adsorption properties of arc produced multi walled carbon

nanotubes for bovine serum albumin. *Int J Chem React Eng* 14: 549–558. https://doi.org/10.1515/ijcre-2015-0160

13. Kopac T, Bozgeyik K (2010) Effect of surface area enhancement on the adsorption of bovine serum albumin onto titanium dioxide. *Colloid Surface B* 76: 265–271. https://doi.org/10.1016/j.colsurfb.2009.11.002
14. Kopac T, Bozgeyik K, Flahaut E (2018) Adsorption and interactions of the bovine serum albumin-double walled carbon nanotube system. *J Mol Liq* 252: 1–8. https://doi.org/10.1016/j.molliq.2017.12.100
15. Brownsey GJ, Noel TR, Parker R, et al. (2003) The glass transition behavior of the globular protein bovine serum albumin. *Biophys J* 85: 3943–3950. https://doi.org/10.1016/S0006-3495(03)74808-5
16. Kundu S, Banerjee C, Sarkar N (2017) Inhibiting the fibrillation of serum albumin proteins in the presence of Surface Active Ionic Liquids (SAILs) at low pH: Spectroscopic and microscopic study. *J Phys Chem* 121: 7550–7560. https://doi.org/10.1021/acs.jpcb.7b03457
17. Binaeian E, Mottaghizad M, Kasgary AH, et al. (2020) Bovine serum albumin adsorption by Bi-functionalized HMS, nitrilotriacetic acid-amine modified hexagonal mesoporous silicate. *Solid State Sci* 103: 106194. https://doi.org/10.1016/j.solidstatesciences.2020.106194
18. Hurrell, Lynch F, Sassenko S, et al. (1998) Iron absorption in humans: bovine serum albumin compared with beef muscle and egg white. *Am J Clin Nutr* 47: 1–7. https://doi.org/10.1093/ajcn/47.1.102
19. Semaghiul B, Mihaela MB, Corina P, et al. (2015) Spectrophotometric method for the determination of total proteins in egg white samples. *Rev Chim* 66: 378–381.
20. Karimi M, Bahrami S, Ravari SB, et al. (2016) Albumin nanostructures as advanced drug delivery systems. *Expert Opin Drug Del* 13: 1609–1623. https://doi.org/10.1080/17425247.2016.1193149
21. Nosrati H, Sefidi N, Sharafi A, et al. (2018) Bovine serum albumin (BSA) coated iron oxide magnetic nanoparticles as biocompatible carriers for curcumin-anticancer drug. *Bioorg Chem* 76: 501–509. https://doi.org/10.1016/j.bioorg.2017.12.033
22. Choi JS, Meghani N (2016) Impact of surface modification in BSA nanoparticles for uptake in cancer cells. *Colloid Surface B* 145: 653–661. https://doi.org/10.1016/j.colsurfb.2016.05.050
23. Elzoghby AO, Samy WM, Elgindy NA (2012) Albumin-based nanoparticles as potential controlled release drug delivery systems. *J Control Release* 157: 168–182. https://doi.org/10.1016/j.jconrel.2011.07.031
24. Kopac T, Bozgeyik K, Yener J (2008) Effect of pH and temperature on the adsorption of bovine serum albumin onto titanium dioxide. *Colloid Surface A* 322: 19–28. https://doi.org/10.1016/j.colsurfa.2008.02.010
25. Yeung KM, Lu ZJ, Cheung NH (2009) Adsorption of bovine serum albumin on fused silica: Elucidation of protein-protein interactions by single-molecule fluorescence microscopy. *Colloid Surface B* 69: 246–250. https://doi.org/10.1016/j.colsurfb.2008.11.020
26. Zhao L, Zhou Y, Gao Y, et al. (2015) Bovine serum albumin nanoparticles for delivery of tacrolimus to reduce its kidney uptake and functional nephrotoxicity. *Int J Pharm* 483: 180–187. https://doi.org/10.1016/j.ijpharm.2015.02.018
27. Mallakpour S, Yazdan H (2018) Ultrasonics-Sonochemistry: The influence of bovine serum

albumin-modified silica on the physicochemical properties of poly(vinyl alcohol) nanocomposites synthesized by ultrasonication technique. *Ultrason Sonochem* 41: 1–10. https://doi.org/10.1016/j.ultsonch.2017.09.017

28. Joseph D, Sachar S, Kishore N, et al. (2015) Mechanistic insights into the interactions of magnetic nanoparticles with bovine serum albumin in presence of surfactants. *Colloids Surf B* 135: 596–603. https://doi.org/10.1016/j.colsurfb.2015.08.022
29. Timin AS, Solomonov AV, Musabirov II, et al. (2014) Immobilization of bovine serum albumin onto porous immobilization of bovine serum albumin onto porous poly(vinylpyrrolidone)-modified silicas. *Ind Eng Chem Res* 53: 13699–13710. https://doi.org/10.1021/ie501915f
30. Ruiz CC, Herrero AM (2019) Impact of biogenic amines on food quality and safety. *Foods* 8: 62. https://doi.org/10.3390/foods8020062
31. Ladero V, Calles-Enríquez M, Fernández M, et al. (2010) Toxicological effects of dietary biogenic amines. *Curr Nutr Food Sci* 6: 145–156. https://doi.org/10.2174/157340110791233256
32. Ahmadi E, Hashemikia S, Ghasemnejad M, et al. (2014) Synthesis and surface modification of mesoporous silica nanoparticles and its application as carriers for sustained drug delivery. *Drug Deliv* 21: 164–172. https://doi.org/10.3109/10717544.2013.838715
33. Cao S, Aita GM (2013) Enzymatic hydrolysis and ethanol yields of combined surfactant and dilute ammonia treated sugarcane bagasse. *Bioresource Technol* 131: 357–364. https://doi.org/10.1016/j.biortech.2012.12.170
34. Jung HS, Moon DS, Lee JK (2012) Quantitative analysis and efficient surface modification of silica nanoparticles. *J Nanomater* 2012:1–8. https://doi.org/10.1155/2012/593471
35. Mallakpour S, Nazari HY (2017) Ultrasonic-assisted fabrication and characterization of PVC-SiO_2 nanocomposites having bovine serum albumin as a bio coupling agent. *Ultrason Sonochem* 39: 686–697. https://doi.org/10.1016/j.ultsonch.2017.05.036
36. Mujiyanti DR, Komari N, Sari NI (2013) Kajian termodinamika adsorpsi hibrida merkapto-silika dari abu sekam padi terhadap ion Co(II). *J Kim Val* 3: 71–75. https://doi.org/10.15408/jkv.v3i2.500
37. Nairi V, Medda S, Piludu M, et al. (2018) Interactions between bovine serum albumin and mesoporous silica nanoparticles functionalized with biopolymers. *Chem Eng J* 340: 42–50. https://doi.org/10.1016/j.cej.2018.01.011
38. Hamdiani S, Nuryono N, Rusdiarso B (2015) Kinetika adsorpsi ion emas(III) oleh hibrida merkapto silika. *J Pijar MIPA* 10: 1–4. https://doi.org/10.29303/jpm.v10i1.11
39. Konicki W, Aleksandrzak M, Mijowska E (2017) Equilibrium, kinetic and thermodynamic studies on adsorption of cationic. *Chem Eng Res Des* 123: 1–6. https://doi.org/10.1016/j.cherd.2017.03.036
40. Lima ÉC, Adebayo MA, Machado FM (2015) Kinetic and equilibrium models of adsorption. In: Bergmann CP, Fernando MM, *Carbon Nanomaterials as Adsorbents For Environmental and Biological Applications*, Berlin: Springer International Publishing, 33–69. https://doi.org/10.1007/978-3-319-18875-1_3
41. Naat JN, Neolaka YAB, Lapailaka T, et al. (2021) Adsorption of Cu(II) and Pb(II) using silica@mercapto(HS@M) hybrid adsorbent synthesized from silica of Takari sand: optimization

of parameters and kinetics. *Rasayan J Chem* 14: 550–560. https://doi.org/10.31788/RJC.2021.1415803

42. Supardi ZAI, Nisa Z, Kusumawati DH, et al. (2018) Phase transition of SiO_2 nanoparticles prepared from natural sand: The calcination temperature effect. *J Phys Conf Ser* 1093: 012025. https://doi.org/10.1088/1742-6596/1093/1/012025
43. Abdel-Rahman LH, Abu-Dief AM, Al-Farhan BS, et al. (2019) Kinetic study of humic acid adsorption onto smectite: The role of individual and blend background electrolyte. *AIMS Mater Sci* 6: 1176–1190. https://doi.org/10.3934/matersci.2019.6.1176
44. Tan KL, Hameed BH (2017) Insight into the adsorption kinetics models for the removal of contaminants from aqueous solutions. *J Taiwan Inst Chem Eng* 74: 25–48. https://doi.org/10.1016/j.jtice.2017.01.024
45. Nguyen H, You S, Hosseini-bandegharaei A (2017) Mistakes and inconsistencies regarding adsorption of contaminants from aqueous solutions : A critical review. *Water Res* 120: 88–116. https://doi.org/10.1016/j.watres.2017.04.014
46. Zhang L, Luo H, Liu P, et al. (2016) A novel modified graphene oxide/chitosan composite used as an adsorbent for Cr(VI) in aqueous solutions. *Int J Biol Macromol* 87: 586–596. https://doi.org/10.1016/j.ijbiomac.2016.03.027
47. Batool F, Akbar J, Iqbal S, et al. (2018) Study of isothermal, kinetic, and thermodynamic parameters for adsorption of cadmium: An overview of linear and nonlinear approach and error analysis. *Bioinorg Chem Appl* 2018: 1–11. https://doi.org/10.1155/2018/3463724
48. Mahmoud NA, Nassef E, Husain M (2020) Use of spent oil shale to remove methyl red dye from aqueous solutions. *AIMS Mater Sci* 7: 338–353. https://doi.org/10.3934/matersci.2020.3.338
49. Wu F, Tseng R, Juang R (2009) Characteristics of Elovich equation used for the analysis of adsorption kinetics in dye-chitosan systems. *Chem Eng J* 150: 366–373. https://doi.org/10.1016/j.cej.2009.01.014
50. Elhafez SEA, Hamad HA, Zaatout AA, et al. (2017) Management of agricultural waste for removal of heavy metals from aqueous solution: adsorption behaviors, adsorption mechanisms, environmental protection, and techno-economic analysis. *Environ Sci Pollut R* 24: 1397–1415. https://doi.org/10.1007/s11356-016-7891-7
51. Neolaka YAB, Supriyanto G, Kusuma HS (2018) Adsorption performance of Cr(VI)-imprinted poly(4-VP-co-MMA) supported on activated Indonesia (Ende-Flores) natural zeolite structure for Cr(VI) removal from aqueous solution. *J Environ Chem Eng* 6: 3436–3443. https://doi.org/10.1016/j.jece.2018.04.053
52. Obradovic B (2020) Guidelines for general adsorption kinetics modeling. *Hem Ind* 74: 65–70. https://doi.org/10.2298/HEMIND200201006O
53. Neolaka YAB, Lawa Y, Naat JN, et al. (2020) The adsorption of Cr(VI) from water samples using graphene oxide-magnetic (GO-Fe_3O_4) synthesized from natural cellulose-based graphite (kusambi wood or Schleichera oleosa): Study of kinetics, isotherms and thermodynamics. *J Mater Res Technol* 9: 6544–6556. https://doi.org/10.1016/j.jmrt.2020.04.040
54. Neolaka YAB, Kalla EBS, Supriyanto G, et al. (2017) Adsorption of hexavalent chromium from aqueous solutions using acid activated of natural zeolite collected from Ende-Flores, Indonesia. *Rasayan J Chem* 10: 606–612. http://dx.doi.org/10.7324/RJC.2017.1021710

55. Edet UA, Ifelebuegu AO (2020) Kinetics, isotherms, and thermodynamic modeling of the adsorption of phosphates from model wastewater using recycled brick waste. *Processes* 8: 665. https://doi.org/10.3390/pr8060665
56. Dizge N, Keskinler B, Barlas H (2009) Sorption of Ni(II) ions from aqueous solution by Lewatit cation-exchange resin. *J Hazard Mater* 167: 915–926. https://doi.org/10.1016/j.jhazmat.2009.01.073
57. Enaime G, Baçaoui A, Yaacoubi A, et al. (2020) Applied sciences biochar for wastewater treatment-conversion technologies and applications. *Appl Sci* 10: 3492. https://doi.org/10.3390/app10103492
58. Zhang L, Luo H, Liu P, et al. (2016) A novel modified graphene oxide/chitosan composite used as an adsorbent for Cr(VI) in aqueous solutions. *Int J Biol Macromol* 87: 586–596. https://doi.org/10.1016/j.ijbiomac.2016.03.027
59. Mustapha S, Shuaib DT, Ndamitso MM, et al. (2019) Adsorption isotherm, kinetic and thermodynamic studies for the removal of Pb(II), Cd(II), Zn(II) and Cu(II) ions from aqueous solutions using Albizia lebbeck pods. *Appl Water Sci* 9: 1–11. https://doi.org/10.1007/s13201-019-1021-x
60. Lim JY, Mubarak NM, Abdullah, et al. (2018) Recent trends in the synthesis of graphene and graphene oxide based nanomaterials for removal of heavy metals–A review. *J Ind Eng Chem* 66: 29–44. https://doi.org/10.1016/j.jiec.2018.05.028
61. Maleki MS, Moradi O, Tahmasebi S (2015) Adsorption of albumin by gold nanoparticles: Equilibrium and thermodynamics studies. *Arab J Chem* 10: S491–S502. https://doi.org/10.1016/j.arabjc.2012.10.009
62. Duranoğlu D, Trochimczuk AW, Beker U (2012) Kinetics and thermodynamics of hexavalent chromium adsorption onto activated carbon derived from acrylonitrile-divinylbenzene copolymer. *Chem Eng J* 187: 193–202. https://doi.org/10.1081/SS-100100208
63. Guibal E, Milot C, Roussy J (2000) Influence of hydrolysis mechanisms on molybdate sorption isotherms using chitosan. *Sep Sci Technol* 35: 1021–1038. https://doi.org/10.1081/SS-100100208
64. Givens BE, Diklich ND, Fiegel J, et al. (2017) Adsorption of bovine serum albumin on silicon dioxide nanoparticles: Impact of pH on nanoparticle–protein interactions. *Biointerphases* 12: 02D404. https://doi.org/10.1116/1.4982598
65. Salis A, Boström M, Medda L, et al. (2011) Measurements and theoretical interpretation of points of zero charge/potential of BSA protein. *Langmuir* 27: 11597–11604. https://doi.org/10.1021/la2024605
66. Li R, Wu Z, Wangb Y, et al. (2016) Role of pH-induced structural change in protein aggregation in foam fractionation of bovine serum albumin. *Biotechnol Rep* 9: 46–52. https://doi.org/10.1016/j.btre.2016.01.002
67. Purtell JN, Pesce AJ, Clyne DH, et al. (1979) Isoelectric point of albumin: Effect on renal handling of albumin. *Kidney Int* 16: 366–376. https://doi.org/10.1038/ki.1979.139
68. Jal PK, Patel S, Mishra BK (2004) Chemical modification of silica surface by immobilization of functional groups for extractive concentration of metal ions. *Talanta* 62: 1005–1028. https://doi.org/10.1016/j.talanta.2003.10.028
69. Abdillah AI, Darjito D, Khunur MM (2015) Pengaruh pH dan waktu kontak pada adsorpsi Ion

Logam Cd^{2+} menggunakan adsorben kitin terikat silang glutaraldehid. *Jurnal Ilmu Kimia Universitas Brawijaya* 1: 826–832.

70. Chaudhry SA, Khan TA, Ali I (2017) Equilibrium, kinetic and thermodynamic studies of Cr(VI) adsorption from aqueous solution onto manganese oxide coated sand grain (MOCSG). *J Mol Liq* 236: 320–330. https://doi.org/10.1016/j.molliq.2017.04.029
71. Bozgeyik K, Kopac T (2010) Adsorption of Bovine Serum Albumin onto metal oxides: Adsorption equilibrium and kinetics onto alumina and zirconia. *Int J Chem React Eng* 8: 1–24. https://doi.org/10.2202/1542-6580.2336
72. Seredych M, Mikhalovska L, Mikhalovsky S, et al. (2018) Adsorption of bovine serum albumin on carbon-based materials. *J Carbon Res* 4: 1–14. https://doi.org/10.3390/c4010003

AIMS Press